Jordanian Journal of Computers and Information Technology (JJCIT), Vol. 08, No. 02, June 2022.

CERVICAL CANCER DETECTION AND CLASSIFICATION USING MRIS

Ichrak Khoulqi and Najlae Idrissi

(Received: 29-Dec.-2021, Revised: 5-Mar.-2022, Accepted: 7-Mar.-2022)

ABSTRACT

Cervical Cancer (CC) is the second most frequent malignancy in women worldwide, with a 60 % mortality rate; it is the leading cause of death worldwide. The majority of cervical cancer deaths occur in less developed countries where there is a lack of screening programs and sensitization about the disease. CC cannot be detected in its early stages, since it does not reveal any symptoms and has a long latent period. Accurate staging can aid radiologists in providing effective therapy by utilizing diagnostic methods such as MRIs. In this paper, two approaches are proposed. The first consists of introducing an automatic system for early detection of CC using image processing techniques and axial, sagittal T2-weighted MRIs for analysis to determine the pathological stage of tumour and identify the real impact of cancer, that will help the patient to be treated with high efficiency and properly. This detection process goes through three major steps; i.e., pre-processing to make the representation of MRIs significant and easy to be analyzed, then segmentation was performed by region growing and geometric deformable techniques to extract the region of interests (ROIs). In the next step, we extract two categories of features based on statistical and transform methods in order to describe our ROIs. At the final step, five classifiers were trained to classify the MRIs into two classes: benign or malign. The second approach aims to increase the performance of pre-trained Deep Convolutional Neural Networks (DCNNs) based on Transfer Learning (TL) used to classify our Female Pelvis Dataset (FP_Dataset) by adopting the stacking generalized method that provides a more efficient and robust classifier. Data augmentation is a pre-processing method applied to our MRIs and a dropout layer is used to prevent networks from overfitting in our small dataset. The results of experiments show that data augmentation and stacking generalization represent an efficient way to improve accuracy rate of classification.

KEYWORDS

Cervical cancer, MRI, Segmentation, Features, DCNNs, Transfer learning, Stacking, Classification.

1. INTRODUCTION

Cervical cancer is ranked 4th among the world's female cancers. About 500 000 cases of cervical cancer [1], 200 000 cases of cancers of the body of the uterus and 200 000 cases of other gynecological cancers, such as ovaries, vulva and vagina, appear each year [1]. In Morocco, uterine cancer is ranked 2nd among female cancers in Moroccan women, with more than 3300 new cases and 2500 deaths per year [2].Cervical cancer is characterized by uncontrolled proliferation of abnormal cells that can invade and damage normal tissue [3]. The majority of cervical cancers originate in the cells that line the cervix. These cells do not transform directly into cancer; instead, normal cells in the uterus progressively develop precancerous changes that can turn into cervical cancer. The incidence of cervical cancer increases with age and reaches a stage from age 50; the main cause of CC is due to a sexually transmitted infection: Human Papillomavirus (HPV).In most cases, this infection is eliminated naturally in about 80% of women and in 10% of women this virus can cause precancerous lesions that can develop into tumours. Other causes that can lead to cancer include smoking, suppression of the body's immune system…etc. As mentioned above, CC has no symptoms. Therefore, as part of prevention, women should perform a Pap Smear test, which is a widely used colposcopy to check the uterine and vagina. This test can identify abnormal and irregular cells on the cervix and helps detect the cancerous tissues at an early stage.

In this work, we will take the following technical route: we will represent the state-of-the-art in the related work section, the proposed approaches, which are divided into two subsections; the first depicts approaches based on image processing techniques and the second on Deep Convolutional Neural Networks (DCNNs), the evaluation of the different proposed approaches in the experimental results section and finally the conclusion.

I. Khoulqi and N. Idrissi are with DICC Team, Data4Earth Laboratory, Sultan Moulay Slimane University, Beni Mellal, Morocco. Emails: ichrak.khoulqi@gmail.com and idrissi.najlae@gmail.com

2. RELATED WORK

MR image interpretation for the diagnosis of female pelvis part is a time-consuming, sensitive and hard complicated task due to different characteristics, such as size, shape and texture. To overcome this problem, two different categories of pre-treating, segmenting and classifying techniques exist.

2.1 Classical Methods

To detect and classify Cervical Cancer (CC), several works have been carried out using colposcopy images to observe cell change and X-ray techniques to analyze tissues and tumour extension in case of their presence. Among these works, we find the following: Bethanney et al. [4] suggested an automatic cervical cancer diagnosis method based on texture descriptors and SVM multiclass classification (Support Vector Machine). Their work is divided into four stages: Pre-treatment, in which MRIs are pre-treated by removing undesired noises and other factors by equalizing the histogram and increasing the contrast, as well as using a nonlocal means filter. In the segmentation phase, the authors used the region growth method to extract ROIs; in the description phase, a gray level co-occurrence matrix was used to extract significant features about ROI texture; and finally, multiclass SVM was used to classify data into non-cancerous, benign and malignant.

Mithlesh et al. [5] work revolves around the use of Pap Smear images to perform automatic approaches to determine the shape, size and texture of the nucleus of the cell; their work is divided into three stages: Pre-processing, segmentation and classification. The Pap Smear images are converted to grayscale and in order to extract the nucleus from the cytoplasm, the borders must be highlighted with contrast enhancement before using the Gaussian filter to reduce noise. To extract the ROI, several thresholds are utilized that vary depending on the input image; the image gradient is calculated to define the boundaries of the nucleus and then the morphological operators are used to clean the segmented image. They extracted the nucleus properties for the classification phase during the description step and the characteristics used are: number of nuclei in the image, area, compactness, major axis, minor axis, aspect ratio and eccentricity. They used the Support Vector Machine to classify their data into three different classes, CIN1, CIN2 and CIN3.

Robert et al. [6] also employed Pap Smear images to construct an automatic detection system in order to eliminate difficulties caused by interpretation under the microscope; their work was divided into four phases: They used a Kernel of 3*3 for pre-processing and to determine the optimal kernel coefficients, they used a genetic algorithm with a repeat of 50 to 100 iterations, followed by a convolution procedure to obtain a noiseless image. After transferring the improved image (RGB) to the HSI space, the segmentation stage employs mathematical morphological operators. In the feature extraction or description step, five features are extracted: energy, local variation, correlation, entropy and homogeneity. Finally, in classification, they used the K-means method to classify the input image as normal or abnormal based on the extracted characteristics.

The work [7] comprises the identification and categorization of cervical cancer utilizing MRI scans, with the following workflow: Preprocessing; this phase allows for the enhancement of MRI image intensities *via* gamma correction and the probability of pixel luminance distribution. Then, the authors adopted Otsu thresholding for segmentation, which was based on thresholding by determining an ideal grey level to separate the ROI from its background. In the feature extraction step, they used gray level co-occurrence, contourlet features and Gabor features matrix. At least, the classification step consists in classifying the data into normal or abnormal based on the Support Vector Machine (SVM) technique. Sajeena et al. [8] proposed an automated method for the identification of cervical cancer by segmenting and classifying cervical cells; their paper is provided in four steps: Image acquisition for Pap Smears, then noise reduction using the non-local means filter to improve the visual quality of the image. Then, the K-means clustering method is used to partition the cell to cytoplasm, nucleus and background and the Radiating Gradient Flow (RGVF) snake is conducted. Six features are calculated from the extracted ROI: Area, compactness, major axis, minor axis, aspect ratio and nucleus homogeneity. Finally, classification is used to classify the data as normal or abnormal, with three different classifiers.

2.2 Deep-learning Methods

The last years, deep-learning model (Convolutional Neural Network) achieved a big success in

analyzing and classifying biomedical images that were being seen in health-care systems for detecting tumours, like lung nodule classification, breast cancer detection, identification of skin disease, …etc. In order to get a stable, fast and accurate model Transfer learning technique is used to improve CNN architecture.

In [12], Almubarak et al. used CNN to classify squamous epithelium into 4 grades of Cervical Intraepithelial Neoplasia (CIN) by dividing the epithelium into 10 segments and each segment into 3 parts (top, middle, bottom); then, they used a Deep Neural Network which consists of 32 filters with limited epochs and obtained a gained accuracy rate of 77,25%. Sun et al. [13] adopted random and hybrid decision tree to classify the cancerous images (Pap Smear images) into two classes: normal or abnormal, where the accuracy rate was 94.4%.

Antonios Makris et al. [14] proposed using Deep Convolutional Neural Networks to classify COVID-19 using a variety of pre-trained models including Xception, InceptionV3, MobileNetV2, VGG16, VGG19 and NasNetLarge. The dataset is divided into three classes: Covid, Normal and Pneumonia, which are classified using chest X-ray images that were split into 80 % and 20% for training and testing, respectively, with 35 epochs, a learning rate of 1e-3 and a batch size of 8.The best accuracy was 95.88% when using VGG16 as a fine-tuned pre-trained model.

The authors of [15] used deep learning to create a diagnostic system for cervical squamous intraepithelial lesions. They collected data to create three deep-learning models. The first step in this work consists of pre-processing data by resizing all images into 512*512 pixels and dividing them into 100 categories by K-means and randomly relocating them into three sets (training set, validation set and test set). The second step is based on transfer learning technique using ResNet pre-trained model on ImageNet dataset to improve the efficiency of the proposed techniques, in order to classify images into two groups. Their proposed approach obtained an accuracy rate of 84.10% with an AUC of 0.93 and for evaluating segmentation, the DICE metric was used and they obtained an average accuracy of 95.59%. The authors proposed two deep-learning CNN architectures to detect cervical cancer based on colposcopy images in [15]. The first is the pre-trained VGG19 model, which achieved an accuracy of 73.3% and the second is CYENET, which achieved an accuracy of 92.3%.

In [9], Saumaya et al. improved and fine-tuned the EfficientNetB3 model to classify malignant skin lesions by comparing several pre-trained models, such as ResNet50, InceptionV3, InceptionResNetV2 and EfficientB0-B2 models. Their proposed model achieved an accuracy of 87.12%, a recall of 87.12%, a precision of 87.12% and an F1-score of 85.12%. In [10], a modified K-means is suggested to extract the region of interest from mammography, followed by textural features retrieved using GLCM and Gabor and CNN features extracted using the pre-trained model InceptionV3 after simple pre-processing and cropping. Cross-validation is used to assess the quality of the retrieved features using five different classifiers; namely, SVM, KNN, MLP, RF and NB.

3. THE PROPOSED APPROACHES

The proposed approaches are presented in this section by explaining each stage of the computer-aided diagnostic system of the first approach that has some objective to finally achieve the obtained results and those can be obtained by adopting and applying different techniques, such as noise removal, filtering and contrast enhancement in the pre-processing step. Similarly, the image segmentation step consists of extracting the ROIs, followed by feature extraction and selection to obtain significant characteristics that better define our ROIs. Finally, we go to the classification step to categorize our female pelvis dataset as malign or benign. Due to a lack of female pelvis MRIs, we chose a deep convolutional neural network with transfer learning as our second strategy in order to increase the learning capability of the suggested model and develop a meta-learner that improves the performance of our proposed model. In the next subsections, we will go through each stage of each proposed approach in further detail.

3.1 First Proposed Approach

To increase the chances and possibilities of detecting cervical cancer in early stages, we have proposed two approaches based on the analysis and interpretation of MRI images. The female pelvis MRIs used in this work are collected from different web sources. In this paper, we worked with two slices of the

pelvic part: axial and sagittal, which allowed us to better visualize the tumour in order to extract it and place it in its most appropriate pathological stage, with the aim of enhancing the chances of survival and healing.

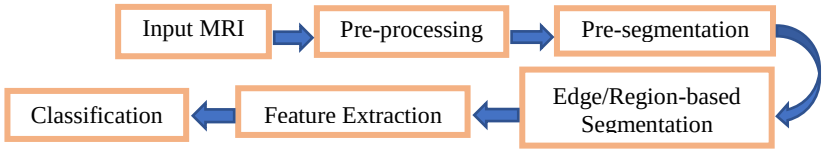

Figure 1. Block diagram of the first proposed system.

Figure 1 depicts the global schema of our first proposed detection system based on image processing techniques taking place in four steps.

1) **Pre-processing:** Denoising and enhancing borders of structures and tissues in order to get a better visual quality of MRI scans for further phases.
2) **Segmentation:** Consists of extracting the region of interests (ROIs) or tumoral zones using two different approaches: Distance Regularized Level Set Evolution (DRLSE) and Region Growing-based Gradient. Those techniques are largely used for image analysis in many fields, such as segmentation of brain tumours using LevelSet evolution [16], automatic detection of man-made objects from aerial and satellite images based on LevelSet evolution [17], automatic image segmentation by integrating color-edge extraction and seeded region growing [18] and adaptive region growing technique using polynomial functions for image approximation [19].
3) **Feature Extraction:** Crucial step for separating beneficial characteristics from the extracted ROIs.
4) **Classification:** Final step of the process of detection and classification by categorizing our female pelvis dataset into malignant or benign.

Detection of cervical cancer is a complicated task that requires high precision in detection to stadify our Female Pelvis MRIs, which is why we have proceeded with a pre-processing step to improve the MRIs quality and then we select our ROIs as is required in the segmentation step using two different approaches as cited above; region-based technique by implementing region growing method, which is simple, fast and computationally inexpensive. The second segmentation strategy was based on boundary or contour to recognize abrupt changes in grayscale images. These algorithms are versatile in recognizing ROIs by respecting their morphology that will help us in further steps.

3.1.1 Pre-processing

MRI images of the pelvic area are altered by a variety of noise leading to inaccuracy in the detection of cervical cancer and this is due to a variety of factors during the process of imaging the pelvis, such as the influence of contrast, temperature and other factors like the technics problem in the machines during the capturing which affects the MRI by a blurring which does not allow a better visualization of the different regions of the pelvis. In order to remedy these alterations and enhance the visual quality of images to be more useful and usable and to increase the efficiency of our different proposed approaches, we have to go through an essential phase which is pre-processing. In this study, it is essential to have information on the edges to be able to retrieve the region of interest (ROI); for example, we have filters such as the averaging filter that smoothes the sudden change in illuminance on the borders, which is not perfect for our case study, so we chose to use a non-linear filter that removes Gaussian noise while keeping the edges, which will give us a clearer image that is easier to analyze and interpret. It is the bilateral filter.

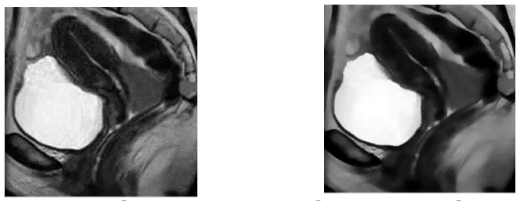

(a) Original image (b) Pre-treated image

Figure 2. Pre-processing phase based on bilateral filter.

Bilateral Filter (BLF) [21]-[22]: The basic idea of this filter is to add weights to the Gaussian convolution taking into consideration the distance between pixels in the illuminance space. This filter is used for noise reduction and image enhancement; this filtering technique is adapted to our MRI images by preserving their disjunctions to separate the images into different regions [16]. It consists in filtering the MRI images of the pelvis while keeping the abrupt change of intensities between the MRI structures (the edges).

Contrast Adjustment

MRI images of the pelvic area are pre-treated with the bilateral filter (BLF) to remove the noise existing in the images while keeping the edges of the different parts composing the pelvis. Then, we move on to another problem that arises when taking MRI scans, which is the contrast. To limit the impact of this problem, we must adjust it to improve the clarity of our data and facilitate the execution of the next steps of our proposed detection system. MRI images are enhanced using an innovative strategy of adjusting the image intensity; the imadjust function is used to transform the intensity of images to enhance the appearance of the pelvis regions for better quantification results. This function is given by $J = imadjust(L, [Low_{in}\ High_{in}], [Low_{out}\ High_{out}], gamma)$ in Matlab [23]; it consists into mapping the intensity values for the input image to new values (J between $Low_{in}\ and\ High_{in}$ mapped to values between $Low_{out}\ and\ High_{out}$); as a default, 1% of the data is immersed at both low and high input image intensities [24]. If gamma is greater than 1, the mapping goes toward dark output values. In this work, gamma value is set to 1 which is the default value and it gives desired results for our MRI data of the pelvis.

Pre-segmentation: Initialization Phase

In the field of cervical cancer detection, the authors proposed in this work [25] an initialization phase before proceeding to the segmentation based on the K-means algorithm. Using this algorithm, we observe that the different structures of the pelvis are better contrasted and the borders of the neighboring structures are clear. For the axial oblique section, it is divided into 5 essential regions (uterus, rectum, bladder, pelvic floor muscles and the tumour if present) as well as for the sagittal section (uterus, ovaries, rectum, acetabulum and the lesion if present).Figure 3 illustrates the results obtained for the pre-segmentation phase.

Segmentation Step

Image segmentation is a critical and crucial step in image analysis, especially for medical images where the information to be extracted is very important and where any loss of information can modify the final decision. It consists of dividing an image into regions or categories, which correspond to different objects or parts of objects. The interest of this segmentation is to be able to manipulate these regions *via* high-level processing [26] to extract their shape characteristics (i.e., distance, position, size, …etc.). Segmentation methods are classified according to two properties: similarity and discontinuity. Based on these properties, image segmentation is defined by two categories: edge-based segmentation and region-based segmentation. The region-based segmentation divides an image into similar areas of connected pixels. In our study, we were based on the region growing method and for edge-based or discontinuity-based techniques, we were based on the regularized distance of level set evolution. In the segmentation step of our proposed detection system, we extract the ROI which is the cervical tumoral zone, the region where the cancer is present and where it has spread too. More details are given in the following sections.

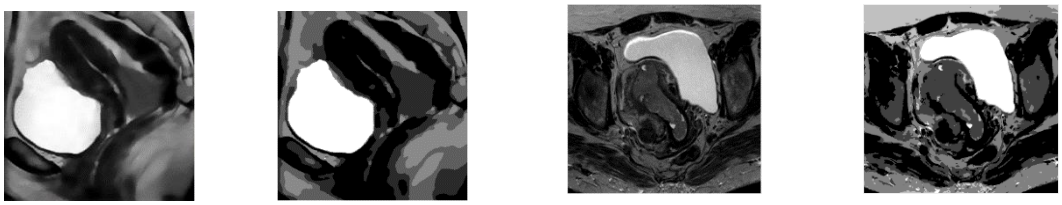

(a) Pre-treated sagittal (b) Initialization (c) Pre-treated axial (d) Initialization

Figure 3. Sagittal and axial image initialization by K-means algorithm.

Geometric Deformable Model

Geometrical method is a model based on the curve evolution technique. The curves are always

evolving towards the normal direction. Geometrical snakes are represented implicitly [24] as the zero-level set of the surfaces with higher dimensions [27]. The update is performed on the surface function in the entire image domain.

Level Set Method (LVS): LVS is presented by Osher and Sethian [28]. It is the surface that intersects the plan and gives us a contour. LVS is the formulation of active contours; this surface is updated with forces derived from the images. In 2D, the curve around the object to be segmented or extracted evolves depending on the internal and external forces.

- **Internal forces:** Defined in the properties of the curve; preservation of the smooth appearance of the curve during its deformation.
- **External forces:** Defined from the image; curve deformation according to the characteristics of the image.

In 3D, the level set (LSF) function incorporates this curve as a zero-level set, which means that it is a surface $\emptyset$ with no height $\emptyset = 0$. Moving fronts are noted by C represented by the zero level $C(t) = \{(x, y)/\emptyset(x, y, t) = 0\}$ of the level set function $\emptyset(x, y, t) = 0$. The main idea of this technique is to place a contour in an image which deforms until it achieves an optimal position and shape. A point $x = (x, y)$ belonging to the front of the surface evolves over time, so we denote by $x(t)$ its position. For each point $x(t)$ on the front has by definition no height, thus:

$$\emptyset(x(t), t) = 0 \tag{1}$$

Level set methods are represented by a partial differential equation (PDE) to determine the position of $\emptyset$ at any time t, where the PDE is as follows:

$$\frac{\partial \emptyset}{\partial t} + F|\nabla \emptyset_t| = 0 \tag{2}$$

The level set method is used to solve several problems in different research fields, such as medical imaging, engineering fields, …etc. The application of LevelSet Standard methods suffers from irregularities of the Level Set Function (LSF) during evolution. The PDE can develop a sharp or flat shape during evolution, which makes the calculations very inaccurate that necessitates a reinitialization; the latter is executed by periodically stopping the evolution and reshaping the degraded LSF as a signed distance function; the distance signed $z = \emptyset(x, y)$ is a surface the plane tangent of which makes an angle of 45° with xy in the plane and the z axis. This condition is verified by the property of the distance signed $|\nabla \emptyset| = 1$ [29]. The disadvantage of a reinitialization is that it affects numerical accuracy, which is why PDE is converted into a variational levelling [30] technique based on energy minimization, useful for adding external shape, color or texture information to the model.

Distance Regularized LevelSet Evolution (DRLSE)

For the segmentation of MRI images of the pelvic part, we use information provided by the edges to determine the external energy; the distance regularization method for the evolution of levelSet (DRLSE) [30] consists in determining a convolution function that smoothes and reduces the noise in the image. This function g always takes minimum values on the edges of an object against other regions. The formula of the convolution function is represented as follows:

$$g \triangleq \frac{1}{1+\nabla G_\sigma * I} \tag{3}$$

where G_σ is the Gaussian kernel with a standard deviation σ and I is the image to be segmented defined on a domain Ω. The definition of functional energy is as follows:

$$\varepsilon(\emptyset) = \mu R_p(\emptyset) + \lambda L_g(\emptyset) + \alpha A_g(\emptyset) \tag{4}$$

where $\mu > 0$ is a constant and $R_p(\emptyset)$ is the term of regularization of level set; its formula is defined as follows:

$$R_p(\emptyset) \triangleq \int p(\nabla \emptyset) dx \tag{5}$$

where p is a potential; $\lambda > 0$ and $\alpha \in R$ are the coefficients of the functional energies $L_g(\emptyset)$ and $A_g(\emptyset)$.

The DRLSE (Distance Regularized Level Set Evolution) approach is used for the segmentation and extraction of the region of interest. In our case study, it shows a great efficiency, since it respects the edges and the geometric shape of the ROI given the high importance of the latter for staging. The

obtained results for segmenting axial and sagittal MRIs of the cervix by the DRLSE are shown in Figure 4 and Figure 5, respectively.

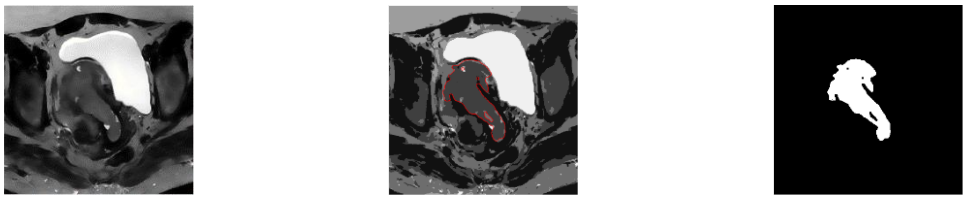

(a) Pre-treated MRI (b) Segmented image (c) Binary image

Figure 4. Segmentation of axial MRI by DRLSE approach.

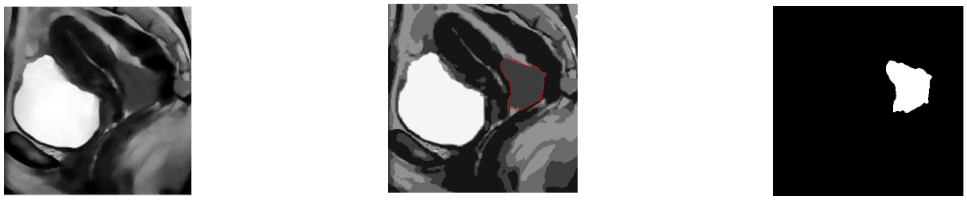

(a) Pre-treated MRI (b) Segmented image (c) Binary image

Figure 5. Segmentation of sagittal MRI by DRLSE approach.

As shown from Figures 4 and 5, the pelvic parts or the suspected tumoral cervix zone is well limited by the red curve as presented in the figures, which delimits and fits too well the cervical tumoral parts to keep only the extracted ROI. As shown in Figures 4 (c) and 5 (c), we apply a simple thresholding to previously segmented images. We can notice from these results that the segmentation of cervical MR images by DRLSE approach gives a good separation of ROI with fine and better localized contours.

Region-based Techniques

Region growing method allows to group in an iterative way connected regions whose union respects a property of homogeneity; it is a tool used for image segmentation introduced by ZUCKER and it has been used repeatedly for the segmentation of medical images [17]. In this paper, new algorithm of segmentation based on the gradient and the seeded region growing for cervical cancer is introduced to extract the malignancy from the MRI images, so first we calculate the gradient of the pre-treated and initialized MRI in order to determine the edges of different parts that compose the MRI perfectly and to avoid the problem of over-segmentation caused by the selection of seed points. There are several edge detection algorithms; the most popular and used are Canny, Sobel and Prewitt. Commonly, the gradient of an image is computed by convolving the image with kernel (filter mask) yielding the image derivatives in x and y directions. The magnitude and direction of the gradient can then be calculated using those derivatives. The region growing technique is our second approach, since it allows us to segment the image well and extract the lesion with precision, always keeping its geometric shape as we have already mentioned in the first approach, since the geometric shape is very important for the next phase (classification). The results of this approach are illustrated in Figures 6 and 7 for axial and sagittal MRI cervix images, respectively.

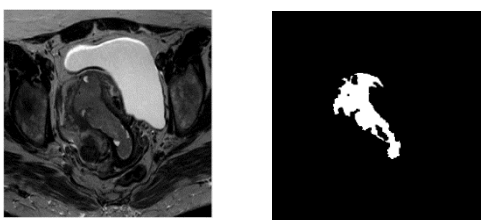

(a) Pre-treated MRI (b) Segmented MRI

Figure 6. Segmentation of axial MRI by RG-based gradient.

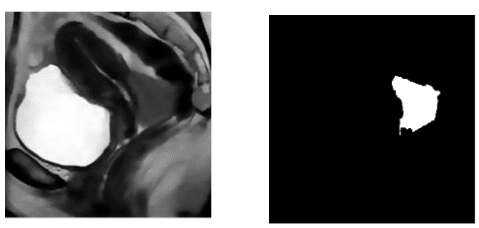

(a) Pre-treated MRI (b) Segmented MRI

Figure 7. Segmentation of sagittal MRI by RG-based gradient.

3.1.2 Feature Extraction

In order to extract beneficial characteristics from the image, we should go through feature extraction

or descriptors, where selecting features helps in the classification, clustering or prediction step by representing our data in a better way .It consists in finding the most compact and informative set of features by measuring properties like color, texture or shape of the whole image or sub-image that is represented in our study by the region of interest (ROI) or the tumoral zone.

During this work, we choose Gray Level Co-occurrence Matrix (GLCM) [31], which is a **statistical tool** that extracts second order texture data from image as texture analysis is well adopted to the monitoring of disease and for characterizing the lesions [32].Also, we proceed to the utilization of Local Binary Pattern (LBP) that characterizes the texture present in the image in the gray levels by attributing to each pixel of the image a value that describes or characterizes the local binary pattern around this pixel [33].Among the approaches of texture analysis, there are techniques based on **transform methods**, such as Discrete Cosine Transform (DCT) [34] that allows the change of the field of study while keeping exactly the same studied function. In our work, we study MRIs; which means a 3-dimensional function: X and Y, indicating the pixel and Z the value of the pixel at this point. The features extracted from the region of interest (ROI) are depicted in the following table.

Table 1. Summary of image features extracted.

Feature	**Feature description**
DCT	a1, a2
LBP	l1, l2, l3, l4, l5, l6, l7, l8, l9, l10
GLCM	g1, g2, g3, g4, g5, g6, g7, g8
MAX	Length of major axis of the extracted ROI
A	Total number of pixels in the ROI
C	Compactness($\frac{P^2}{A}$), where P is the perimeter and A is the area of the ROI

3.1.3 Classification Step

Classification plays an important role in medical applications. In this section, we have outlined the classification of cervical cancer. The CC detection is a very challenging task as this cancer occurs without revealing any symptoms. In this paper, five classifiers including **Random Forest (RF)** [35], **Artificial Neural Network (ANN)** [36], **Decision Tree (DT)** [37], **K-nearest neighbour (KNN)** [38] and **Gradient boosted tree (GBT)** [39] are applied to figure out the appropriate classification of our data. Before the step of classification, we should go through the normalization, because it makes data have the same scale, so each extracted feature is equally important; if we forget to normalize, one of our features might completely dominate others. In our case, we choose using **Z-score normalization** by adopting the following formula:

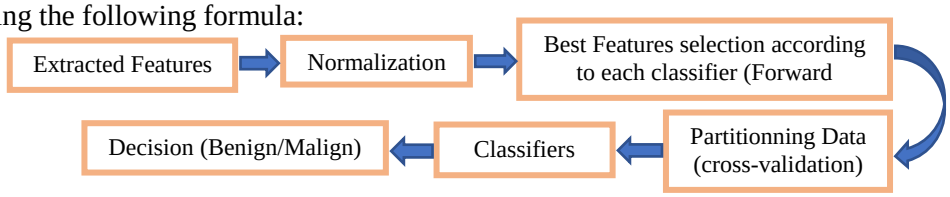

Figure 8. Block diagram of the proposed approach of classification.

$$Z_{score} = \frac{value - \mu}{\sigma} \quad (6)$$

where μ is the mean value of the feature and σ is the standard deviation of the feature. This technique shows a good result, as it can handle outliers. The schema below depicts the CC classification process.

3.2 Approaches to Classification-based Deep Learning

The second proposed approach is based on Convolutional Neural Networks (CNNs). It consists of adopting an ensemble model [46] designed by collaborating six different transfer learning techniques; i.e., NasNetLarge, Xception, VGG16, ResNet152V2, MobileNetV2 and InceptionResNetV2. Ensemble learning leads to augment the classification rate, which leads us to get a powerful approach by remedying the problem caused by the high variance that occurs from the stochastic nature of the neural networks in training. The ensemble learning approach proposed in this work is called stacking generalization or stacking, where a new model learns how to better combine the predictions from the different sub-models. It enhances the learning system's generalization ability; the base learners or

classifiers can be chosen or generated in two manners: The dataset is identical to the various learning algorithms (heterogeneous learners) or the other way around (homogenous learners). The stacking procedure goes through two steps:

- **Level 0:** learns to make predictions from training dataset (inputs).
- **Level 1:** takes the outputs of the proposed sub-models as input and the meta-learner makes predictions from this data.

3.2.1 Convolutional Neural Networks

CNN models perform in a better way in various domains, such as industry, agriculture, detection and classification of medical diseases. The conception or the architecture of CNNs clones the visual cortex system of humans [48]-[49]. It consists of three main steps; the first is convolutional layers, the second is the pooling layer and finally the fully connected layer that are mandatory layers; the secondary layers are depicted by the dropout layer which is used to overcome overfitting during training and the normalization layer; those layers are exploited to increase CNN model performance. The two first layers (convolutional and pooling layers) are in charge of learning to extract the essential features by applying a window size named kernel that convolves the image to extract significant and important features that will be used in the classification tasks and the last one (fully connected layer=FC) does the classification.

In this paper, we took six different types of Deep Convolutional Neural Networks (DCNNs) as cited above that have been pre-trained on natural image dataset (ImageNet) whose weight is used in Transfer Learning experiments. The Softmax function is implemented at the final layer (FC) to output the predicted probabilities to determine the class of the female pelvis MRIs.

3.2.2 Transfer Learning

It is often difficult to get a large dataset in the medical Imaging field; the data for CC_MRIs is much lesser. DCNNs cannot learn in a better way the small Dataset; it requires a huge one to train the model in order to provide better results. DCNNs with small dataset lead to overfitting; it occurs when the noise of data is captured by the model and it arises when this latter fit the data too well due to small dataset. All these problems can be resolved by Transfer Learning (TL) techniques.TL uses pre-trained DCNNs in two ways; first, they are used for feature extraction and then the important knowledge is guarded and used by another model designed for classification. The second one is a more sophisticated technique, where some specific modifications are made to the pre-trained model to achieve good results. These modifications include architecture and hyper parameter adjustment. It is important to use the knowledge gained when we solve a problem of natural image recognition to solve different problems of medical image classification. TL or fine tuning is used to enhance the efficiency of DCNNs as cited above; it comprises removing the last fully connected layer of the pre-trained model on ImageNet, since the outputs are 1000 classes to adapt them to our desired output (two classes= malign/benign).

In this proposed approach, we use Adamx optimizer and the categorical cross-entropy loss function to train the model on our MRIs.We adopt this TL technique, because our female pelvis dataset is small and this latter will help us in improving classification rate to get an efficient model of female pelvic MRI classification. To treat the lack of screening MRIs, we use an important technique which aids in enhancing our dataset; it is data augmentation.

3.2.3 Data Augmentation

Data augmentation is the most common method that reduces overfitting. It is used to artificially expand the size of dataset by creating modified versions of MRIs to improve the ability of the fit models to generalize what they have learned from new images. In this paper, the approach of augmentation is a pre-processing step, which means a geometrical transform of the image, such as random flip horizontally and vertically, random rotation within 45°, horizontal shear within 0.2 times, the image width, height and zoom within 0.2 times.

3.2.4 Methodology of the Second Proposed Approach

The scheme in (Figure 9), illustrated a diagram of the second proposed pipeline by presenting how we stacked different machine learning algorithms to improve the prediction rate for FP_Dataset.

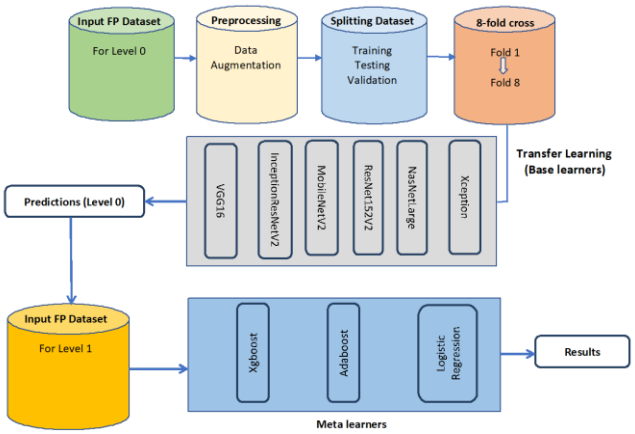

Figure 9. The second proposed pipeline's detailed system.

The following algorithm summarizes the different steps of our proposed approach for FP_Dataset classification.

Algorithm1: Pseudo-code of the Stacking Generalization based Cervical Cancer Classification

Input: Training FP_Dataset with Malignant and Begnin cases D= { (x_1, c_1),(x_1, c_1), …. , (x_n, c_n)}
Base level classifiers $C_1, \dots, C_k$
Meta level classifiers $\hat{C}_1, \hat{C}_2, \hat{C}_3$
Output: Trained ensemble classifiers $\widehat{M}_1, \widehat{M}_2, \widehat{M}_3$
BEGIN
Step1: Train base learners by applying classifiers C_i to FP_Dataset.
for i=1, …, k **do**
$B_i = C_i(D)$
end for
Step 2: Construct new Dataset of predictions $\widehat{D}$
for j=1, …., n do
for i=1, …, k do
% use B_i to classify training sample x_j
$z_{ij} = B_i(x_j)$
end for
$\widehat{\boldsymbol{D}}$= **{**Z_j, c_j**}**, where Z_j= $\{z_{1j}, z_{2j}, \dots, z_{nj}\}$
end for
Step 3: Train a Meta level classifiers
$\widehat{\boldsymbol{M}}_1$=$\hat{C}_1(\widehat{\boldsymbol{D}})$
$\widehat{\boldsymbol{M}}_2$=$\hat{C}_2(\widehat{\boldsymbol{D}})$
$\widehat{\boldsymbol{M}}_3$=$\hat{C}_3(\widehat{\boldsymbol{D}})$
Return $\widehat{\boldsymbol{M}}_1, \widehat{\boldsymbol{M}}_2, \widehat{\boldsymbol{M}}_3$

In the following paragraphs, we provide a summary of the different deep convolutional neural Networks used in this paper.

Xception: The Xception network was introduced by Chollet in 2017 [47]. It is a DCNN that stretches the inception concept to extremes; it introduces new inception layers that are created by depth-wise convolutions that are alternatives to classical convolutions and much more efficient in terms of computation times. The input format of images is 299*299. This network has a depth of 126 with 36 convolutional layers to extract features and a global average pooling layer is adopted to replace the fully connected layers in order to reduce the number of parameters. Then, the activation function Softmax is used to output predictions.

VGG16: VGG16 is a DCNN proposed by K. Simonyan and A. Zisserman (the visual geometry group). It has a depth of 16 [40] weight layers; it achieves an excellent accuracy on the ImageNet classification and on image recognition dataset. The input images format is 224*224, then the filters of 3*3 are applicated in all convolutional layers in order to reduce the number of parameters.

MobileNetV2: MobileNetV2 is an architecture proposed by Google to run on mobiles and an

embedded system [11]. In order to reduce the trainable parameter number, depth-wise separable convolutions are adopted in MobileNet architecture. Depth-wise separable convolution divides the kernel into two small kernels; one for depth-wise convolution and the other for point-wise convolution. This technique of dividing kernels helps in reducing the computational cost. In this work, the pre-trained MobileNet model on ImageNet dataset is imported. It uses an input image of 224*224 and a depth of 88.

InceptionResNetV2: InceptionResNetV2 is an architecture based on InceptionV3 [12] and Microsoft's ResNet [13]-[14]. It combines the properties of both. This architecture is used as a high-level feature extractor which provides information about the image content that can help to characterize the information contained in our MRIs to better classify them. This model is adopted for extracting features and for classification. It has an input image format of 299*299 and a depth of 572.

NasNetLarge: NASNet architectures can be tuned using the reinforcement learning search method by introducing a new concept of normal cell and reduction cell. The NasNetLarge architecture is designed specifically to train on large datasets. Since training on large datasets is expensive and resource-intensive, the search for an architectural block is performed on a small dataset and then the block is transferred to a larger dataset using the NASNet search space. The key aspect of NasNetLarge includes the **ScheduledDropPath** regularization technique that significantly improves the generalization of NASNet models.

ResNet152V2: Residual Networks (ResNet) [50] were proposed as a family of multiple deep neural networks with similar structures, but with different depths. ResNet introduces a structure called residual learning unit to alleviate the degradation of deep neural networks. The main merit of this unit is that it produces better classification accuracy without increasing the complexity of the model. The difference between ResNet152V2 and the original V1 is that V2 uses batch normalization before each weight layer. In the field of image recognition, it has a strong performance that justifies our selection among ResNet by Resnet152V2 as it achieves the best accuracy.

We have modified the pre-trained architectures of Xception, VGG16, MobileNetV2, InceptionResNetV2, NasNetLarge and ResNet152V2 by adding dense layers with ‘relu’ activation, dropout and SoftMax layers with two outputs (malign/begnin). We implement our methods using Keras library and Tensorflow. For our experiments, we load weights of the pre-trained CNNs given by Keras. In the following part, we focus on machine-learning algorithms adopted as Meta learners to increase the classification rate.

Adaptative Boosting: Adaptative boosting (Adaboost for short) algorithm is a technique used as an ensemble method in machine learning. The reason behind the name of this algorithm is that the weights are re-assigned to each instance by attributing higher weights to incorrectly classified instances. It is used to reduce bias as well as variance for supervised learning. As we said above, the main idea is to give more importance to the misclassified data points built by the first weak learner and then construct another weak learner based on the incorrectly classified data. The following formula represents the Adaboost algorithm:

$$F(x) = sign(\sum_{k=1}^{K} \theta_k f_k(x)) \tag{7}$$

where, K: weak classifiers’ number, θ: Weight of k-th weak classifier and $f_k(x)$: weak classifier.

Logistic Regression: Logistic regression is a linear model with binary output; it models the variable with a line for two dependent variables or hyperplane in case of more than two variables. The logistic operation is as follows:

$$p = \frac{1}{1+e^{-(\beta_0+\beta_1 x_1+\cdots+\beta_n x_n)}} \tag{8}$$

where, p: the probability of success (the presence of malignancy), β_0: the model intercepts and β_i: the regression coefficients.

eXtreme Gradient Boosting: eXtreme Gradient Boosting (XGB for short) is one of the approaches to construct ensemble-learning models. It is a tree ensemble model that is represented by a set of classification and regression trees (CARTs). The mathematical formula can be written in the following form:

$$\hat{y}_i = \sum_{k=1}^{K} f_k(x_i) \tag{9}$$

where, K: the trees number, f: Function in functional space F and F: Set of all possible CARTs.

The objective function that needs to be optimized (minimized) can be represented as follows:

$$obj(\theta) = \sum_i^n l(y_i, \hat{y}_i) + \sum_{k=1}^K \Omega(f_k) \quad (10)$$

where, $l(y_i, \hat{y}_i)$: training loss function and $\Omega(f_k)$: regularized term.

4. EXPERIMENTAL RESULTS

4.1 Evaluation of Classical Methods

To evaluate the performance of our computer-aided diagnostic system for cervical cancer (CC) detection and classification, we proceed by evaluating the segmentation and classification proposed techniques.

4.1.1 Quantitative and Qualitative Evaluation of Segmentation

The segmentation process is critical and must be completed appropriately by delimiting the target ROI. To validate this, we begin with a visual inspection, as illustrated in Figure 10. Respectively, the figure represents the segmentation of axial and sagittal MRI cervix images. The first column (a) represents the original cervix images to be segmented, while columns (b) and (c) represent the segmented images obtained by using KM-DRLSE and KM-RG, respectively.

As reported previously, the two approaches give better segmentation by respecting and keeping well the geometric shape of ROI, although the region growing approach outperforms the DRLSE method by specifying the fine details of ROI structure as well as the affected tissues. The second evaluation relies on numerical evaluation based on SSIM (the structural similarity measure [42]) and ZSI (the Zijdenbos similarity index [43]) parameters.

The measurements obtained for these two indices are given in the following table.

Table 2. Evaluation of segmentation approaches.

Experiments	DRLSE		RG	
	SSIM	ZSI	SSIM	ZSI
Experiment 1	0,9429	0,8840	0,9306	0,8067
Experiment 2	0,9863	0,7629	0,9845	0,5756
Experiment 3	0,9535	0,8948	0,9524	0,8726
Experiment 4	0,9359	0,8434	0,9269	0,7846
Experiment 5	0,9700	0,8889	0,8684	0,8684
Experiment 6	0,9664	0,7479	0,9650	0,7386

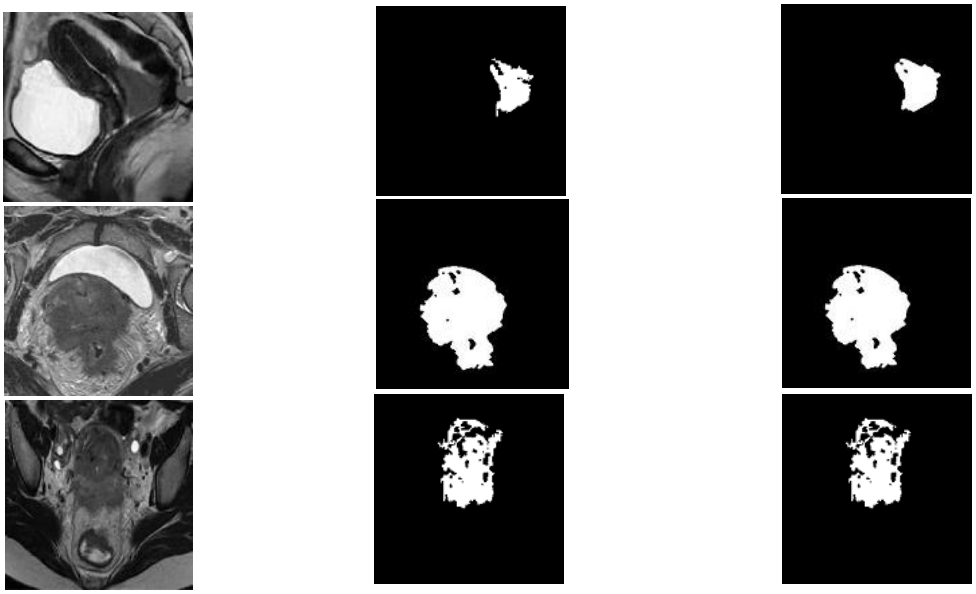

(a) Original MRI (b) Segmented MRI by KM-DRLSE (c) Segmented MRI by KM-RG

Figure 10. Segmentation results by the proposed approaches.

SSIM and ZSI are close to one, indicating better segmentation accuracy. Table 2 shows the results obtained by using the cited evaluation metrics based on the proposed approaches KM-DRLSE and KM-RG. All of the similarity measures produce significant results for all of the values, but as shown in the table, KM-DRLSE outperforms KM-RG, indicating that KM-DRLSE is a powerful technique for extracting a tumoral zone from pelvic MRIs.

4.1.2 Evaluation of Classification

In this sub-section, we will evaluate the classification of pelvic MRIs. After selecting the best feature for each classifier, we proceed to the step of determining the measure ratings in order to assess classification. The results obtained for classification based on KM-DRLSE and KM-RG, respectively, are represented in Tables 3 and 4.

Table 3. Evaluation of classification using KM-DRLSE.

Classifier / Performance	RF	GBT	KNN	DT	ANN
Accuracy	93,103%	93,103%	89,66%	86,21%	86,21%
Recall	90%	80%	90%	80%	90%
Specificity	94,74%	100%	89,47%	89,47%	84,21%
Precision	90%	100%	81,82%	80%	75%
F-measure	90%	88,89%	85,71%	80%	81,82%

Table 4. Evaluation of classification using KM-RG.

Classifier / Performance	RF	GBT	KNN	DT	ANN
Accuracy	79,31%	79,31%	86,21%	86,21%	86,21%
Recall	60%	60%	60%	80%	80%
Specificity	89,47%	89,47%	100%	89,47%	89,47%
Precision	75%	75%	100%	80%	80%
F-measure	66,67%	66,67%	75%	80%	80%

The RF and GBT classifiers perform the best in the approach based on KM-DRLSE with 93,103% of accuracy, while the approach based on KM-RG gives us a good result by using ANN, DT and KNN classifiers.

4.2 Evaluation of the Second Proposed Approach

In this sub-section, we evaluate the second proposed approach adopted to classify FP_Dataset by representing our experimental results.

Cross-validation is a method of evaluation consisting in preventing overfitting and improving the model performance during evaluation. We evaluated the classification performance of the fine-tuned DCNNs with eight-fold cross-validation. This technique allows testing all of the datasets each with a total of eight verifications, which means that the 8^{th} group is used for validation and the other seven groups combined are used for training. To provide comparable results, the same eight training and testing sets were kept in each method.

4.2.1 Evaluation Metrics

To quantify the model's classification performance, evaluation metrics are used. Confusion matrix (CM) was employed, which included accuracy, precision, recall, specificity and F1-score. We calculate the following quantities while evaluating these measures: True Positive (TP), False Negative (FN), True Negative (TN) and False Positive (FP).

After loading the image into the Python Image Library (PIL) format, we convert the PIL image into a Numpy array and we prepare inputs of shape (3,224,224), (3,299,299) and (3,331,331) according to each pre-trained CNN using Keras tools of pre-processing.

Table 5 displays the averages of all evaluation metrics for the various convolutional neural network architectures used in our experiments. We can see that fine-tuned ResNet152V2 outperforms the other

Table 5. The averages of evaluation metrics achieved by each classifier during training and validation using the FP dataset (FP_Dataset).

	Fold	Accuracy %	Recall %	Specificity %	Precision %	F1-measure%
Xception	1	61,53	86,88	25,58	60,50	57,25
	2	66,34	68,85	62,79	66,74	66,48
	3	75,96	88,52	58,13	76,29	75,19
	4	80,58	86,88	71,42	80,48	80,40
	5	81,55	95,08	61,90	82,97	80,75
	6	86,40	93,44	76,19	86,62	86,20
	7	90,29	93,44	85,71	90,28	90,25
	8	88,34	95,08	78,57	88,64	88,17
Average		**71,18**	**77,66**	**61,83**	**71,50**	**70,93**
Standard Deviation		**9,70**	**8,11**	**17,30**	**9,97**	**10,63**
VGG16	1	66,99	93,44	28,57	69,38	62,49
	2	83,49	85,24	80,95	83,56	83,52
	3	87,37	83,60	92,85	88,38	87,47
	4	92,23	91,80	92,85	92,35	92,25
	5	89,32	95,08	80,95	89,51	89,19
	6	93,20	90,16	97,61	93,73	93,24
	7	94,17	1	86,04	94,70	94,09
	8	92,23	96,66	86,04	92,39	92,16
Average		**87,37**	**79,62**	**80,73**	**88,0**	**86,80**
Standard Deviation		**8,37**	**30,01**	**20,48**	**7,78**	**9,75**
InceptionResNetV2	1	73,78	98,36	38,09	79,69	70,46
	2	85,43	90,16	78,57	85,39	85,34
	3	88,34	91,80	83,33	88,32	88,30
	4	93,20	90,16	97,61	93,73	93,24
	5	93,20	95,08	90,47	93,19	93,19
	6	92,23	98,36	83,33	92,67	92,11
	7	91,26	91,66	90,69	91,30	91,27
	8	94,17	98,33	88,37	94,37	94,12
Average		**88,95**	**94,23**	**81,30**	**89,83**	**88,50**
Standard Deviation		**6,34**	**3,48**	**17,21**	**4,77**	**7,35**
MobileNetV2	1	73,04	80,88	61,70	72,76	72,76
	2	82,60	89,70	72,34	82,63	82,38
	3	81,73	88,23	72,34	81,68	81,54
	4	82,60	86,76	76,59	82,53	82,54
	5	84,34	82,35	87,23	85,02	84,45
	6	91,30	92,64	89,36	91,30	91,30
	7	96,52	98,52	93,61	96,55	96,50
	8	93,04	97,01	87,50	93,17	92,99
Average		**85,64**	**89,51**	**80,08**	**85,70**	**85,55**
Standard Deviation		**7,06**	**5,93**	**10,27**	**7,14**	**7,14**
NASNetLarge	1	60	69,11	46,80	59,50	59,68
	2	65,21	55,88	78,72	69,38	65,26
	3	67,82	57,35	82,97	72,50	67,82
	4	78,26	94,11	55,31	79,94	77,06
	5	87,82	91,17	82,97	87,79	87,78
	6	86,95	94,11	76,59	87,24	86,75
	7	92,17	92,64	91,48	92,21	92,18
	8	94,78	97,05	91,48	94,80	94,76
Average		**79,12**	**81,42**	**75,78**	**80,41**	**78,91**
Standard Deviation		**12,45**	**16,47**	**15,26**	**11,56**	**12,49**
ResNet152V2	1	70,19	74,19	64,28	70,31	70,24
	2	91,34	90,16	93,02	91,57	91,38
	3	91,34	95,08	86,04	91,40	91,29
	4	91,34	100	79,06	92,45	91,13
	5	92,30	88,52	97,67	93,02	92,35
	6	94,17	98,36	88,09	94,37	94,12
	7	94,17	95,08	92,85	94,17	94,17
	8	98,05	100	95,23	98,11	98,05
Average		**90,36**	**92,67**	**87,03**	**90,675**	**90,34**
Standard Deviation		**7,91**	**8,03**	**10,20**	**7,95**	**7,89**

proposed five models with 90.36% average accuracy. Data augmentation helps and facilitates the DCNNs to learn the underground feature without the impact of rotation and scale; complicated transforms are not better due to the introduction of noise during feature extraction that leads to disturbing the learning process. The proposed stacked models have performed the best out of the state-of-the-art pre-trained models. As a result, the proposed models have achieved accuracies of 99.56%, 98.70% and 99.56% for XGB, Logistic Regression and AdaBoost as meta-learners, respectively. The suggested model's validity is justified by the values of recall, specificity, precision, F-measure and AUC, as shown in Table 6.

Table 6. Model's validity.

	Accuracy	**Recall**	**Specificity**	**Precision**	**F1-score**	**AUC**
Xception	88,79	92,70	83,15	88,79	88,73	0,87
VGG16	95,25	98,54	90,52	95,37	95,22	0,94
InceptionResNetV2	93,53	100	84,21	94,17	93,42	0,92
MobileNetV2	94,82	97,81	90,52	94,90	94,79	0,94
NasNetLarge	94,39	95,62	92,63	94,39	94,39	0,94
ResNet152V2	95,25	98,54	90,52	95,37	95,22	0,94
XGB	**99,56**	**100**	**98,94**	**99,57**	**99,56**	**0,99**
Logistic Regression	**98,70**	**100**	**96,84**	**98,73**	**98,70**	**0,98**
AdaBoost	**99,56**	**99,27**	**100**	**99,57**	**99,56**	**0,99**

Fine-tuned deep convolutional neural network architectures will produce better results, because they require less computation time than training a DCNN from scratch, allowing it to converge faster.

The base learners required about ten minutes for training purposes. All of the pre-trained models used to identify our female pelvis MRIs achieved the highest accuracy value; nevertheless, given the importance of detecting cervical cancer at early stages, efforts can be made to improve the sensitivity, precision and accuracy scores. As a result, meta-learners are proposed. The proposed models utilizing stacking generalization outperform the base models with 99.56 %, 98.70 % and 99.56 % accuracy for XGB, LR and Adaboost, respectively, which is about 4% higher and an increased precision value, implying the correctness of the predicted results. The results show that the proposed stacking generalized approach yields a high specificity rate, signifying no false positive predictions. The system is more reliable when the specificity is high.

Table 7. Hyper-parameter values.

Hyperparameters	**values**
Learning rate	0.00005
Optimizer	Adam
Batch size	32
Epochs	5

During the training process, the various hyperparameters used in this work were fixed. With a learning rate of 0.00005 and Adam as the optimizer, the batch size and epochs were set to 32 and 5, respectively, as cited in Table 7.

Table 8. Comparative analysis between state-of-the-art and the proposed models.

State-of-the-art	**Accuracy %**	**Precision%**	**Recall%**	**F1-score%**	**AUC**
ML algorithms (DT, RF, XGB) [52]	DT : 93,33%	80	100	89	-
	RF : 93,33%	100	75	86	-
	XGB : 93,33%	0	0	0	-
ML algorithms, Majority Vote [51]	94%	97%	97%	-	0,97
DenseNet121 and The Mutation-based Atom Search Optimization (MASO) algorithm [53]	98,38%	98,58%	99,3%	98,25%	-
Proposed Ensemble Model 1:XGB	**99,56**	**99,57**	**100**	**99,56**	**0,99**
Proposed Ensemble Model 2:Logistic Regression	**98,70**	**98,73**	**100**	**98,70**	**0,98**
Proposed Ensemble Model 3:AdaBoost	**99,56**	**99,57**	**99,27**	**99,56**	**0,99**

4.2.2 Comparative Analysis

The experimental results show that the suggested ensemble models provide a significant rapid and effective solution in the cervical cancer detection field utilizing MRIs of female pelvis. Table 8 compares the performance of existing models to that of the proposed models. The lack of data to train the models leads to models that are poor at generalization. To resolve this concern, we employed transfer learning, which reuses models trained on large datasets, such as ImageNet. We also attempted to make as minimum as possible false predictions. Considering the statistics presented in Table 6, the suggested ensemble models achieve better generalization and less false predictions by beating state-of-the-art models.

5. CONCLUSIONS

To sum up, this article presents two different axes to detect and classify cervical cancer using MRIs, the first based on image processing techniques passing through three essential steps: pre-processing, segmentation and classification of pelvic MRIs. To realize this objective, we propose also two different techniques of segmentation and a variety of descriptors and classifiers that show a high efficiency in extracting regions of interest (ROIs) confirmed due to the obtained values of the parameters of evaluation (ZSI and SSIM) that are close to 1, which means a better segmentation, followed by description and classification into benign or malignant. The experiments performed on our female pelvis dataset approve that the powerful approach of segmenting ROIs is based on KM-DRLSE and Random Forest (RF) for the classification process after using the forward selection to pick only the most informative descriptors. The second axe uses deep transfer learning techniques to build classification models for classifying cervical cancer. Data augmentation pre-processing was performed to enhance our female pelvis dataset to overcome overfitting issues and six pre-trained models are employed. The accuracy rates obtained from Model1, Model2 and Model3 with 99.56%, 98.70%and 99.56%, respectively, show that the proposed ensemble models are capable of detecting CC.

REFERENCES

[1] C. Xavier, J. Levêque and D. Riethmuller,"Cancers Gynécologiques Pelviens," ISBN: 978-2-294-72937-9, Elsevier Masson, 2013.

[2] E. Belglaiaa and C. Mougin, "Le cancer du col de l'utérus: état des lieux et prévention au Maroc," Bulletin du Cancer, vol. 106, no. 11, pp. 1008-1022, 2019.

[3] American Cancer Society, "Cervical Cancer," [Online], Available: https://www.cancer.org/cancer/cervical-cancer/about/key-statistics.html, February 2017.

[4] J. Bethanney, G. Umashankar, D. Sindu and N. Basilica, "Classification of Cervical Cancer from MRI Images Using Multiclass SVM Classifier," International Journal of Engineering and Technology (UAE), vol. 7, no. 2, DOI: 10.14419/ijet.v7i2.25.12351, 2018.

[5] M. Arya, N. Mittal and G. Singh, "Cervical Cancer Detection Using Segmentation on Pap Smear Images," Proc. of the International Conference on Informatics and Analytics (ICIA-16), pp. 1-5, DOI: 10.1145/2980258.2980311, 2016.

[6] P. Robert and A. Celine Kavida, "Classification of Microscopic Cervical Cancer Images Using Regional Features and HSI Model," IJITEE Journal, vol. 8, no. 8S, pp. 24-28, June 2019.

[7] K. Sneha and C. Arunvinodh, "Cervical Cancer Detection and Classification Using Texture Analysis," Biomedical and Pharmacology Journal, vol. 9, no. 2, pp. 663-671, 2016.

[8] T. A. Sajeena and A. S. Jereesh, "Automated Cervical Cancer Detection through RGVF Segmentation and SVM Classification," Proc. of the IEEE International Conference on Computing and Network Communications (CoCoNet), DOI: 10.1109/CoCoNet.2015.7411260, Trivandrum, India, 2015.

[9] S. R. Salian and S. D. Sawarkar, "Melanoma Skin Lesion Classification Using Improved Efficientnetb3," Jordanian J. of Computers and Inf. Technology (JJCIT), vol. 8, no. 1, pp. 45-56, 2022.

[10] T. G. Debelee, A. Gebreselasie, F. Schwenker, M. Amirian and D. Yohannes, "Classification of Mammograms Using Texture and CNN Based Extracted Features", Journal of Biomimetics, Biomaterials and Biomedical Engineering, vol. 42, pp. 79-97, 2019.

[11] M.Sandler, A.Howard, M.Zhu, A.Zhmoginov and L.Chen, "Mobilenetv2: Inverted residuals and linear bottlenecks", Proc. of the IEEE Conf. on Computer Vision and Pattern Recog, pp. 4510-4520, 2018.

[12] H. A. Almubarak, R. J. Stanley, R. Long et al., "Convolutional Neural Network Based Localized Classification of Uterine Cervical Cancer Digital Histology Images," Procedia Computer Science, vol. 114, pp. 281–287, 2017.

[13] G. Sun, S. Li, Y. Cao and F. Lang, "Cervical Cancer Diagnosis Based on Random Forest," International Journal of Performability Engineering, vol. 13, pp. 446–457, 2017.
[14] A. Makris, I. Kontopoulos and K. Tserpes, "COVID-19 Detection from Chest X-Ray Images Using Deep Learning and Convolutional Neural Networks," Proc. of the 11th Hellenic Conference on Artificial Intelligence, DOI: 10.1101/2020.05.22.20110817, 2020.
[15] C. Yuan, Y. Yao, B. Cheng et al., "The Application of Deep Learning Based Diagnostic System to Cervical Squamous Intraepithelial Lesions Recognition in Colposcopy Images," Scientific Reports, vol. 10, article ID: 11639, DOI: 10.1038/s41598-020-68252-3, 2020.
[16] S. Ho, E. Bullitt and G. Gerig, "Level-set Evolution with Region Competition: Automatic 3-D Segmentation of Brain Tumors," International Conference on Pattern Recognition, vol. I, pp. 532-535, Chapel Hill, NC 27599, USA.
[17] K. Karantzalos and D. Argialas, "A Region-based Level Set Segmentation for Automatic Detection of Man-made Objects from Aerial and Satellite Images," Photogrammetric Engineering & Remote Sensing, vol. 75, no. 6, pp. 667–677, June 2009.
[18] J. Fan, D. K. Y. Yau, A. K. Elmagarmid and W. G. Aref, "Automatic Image Segmentation by Integrating Color-edge Extraction and Seeded Region Growing," IEEE Transactions on Image Processing, vol. 10, no. 10, pp. 1454-1466, DOI: 10.1109/83.951532, 2001.
[19] M. Kocher and R. Leonardi, "Adaptive Region Growing Technique Using Polynomial Functions For Image Approximation," Signal Processing, vol. 11, no. 1, pp. 47-60, 1986.
[20] S. Saladi and N. Amutha Prabha, "Analysis of Denoising Filters on MRI Brain Images," International Journal of Imaging Systems and Technology, vol. 27, no. 3, pp. 201-208, 2017.
[21] C. Tomasi and R. Manduchi, "Bilateral Filtering for Gray and Color Images," Proc. of the IEEE 6 th Int. Conf. on Computer Vision (IEEE Cat. No.98CH36271), pp. 839-846, Bombay, India. 1998.
[22] S. Paris and F. Durand, "Fast Approximation of the Bilateral Filter Using a Signal Processing Approach," Proc. of European Conf. on Computer Vision (ECCV 2006), vol. 3954, pp. 568-580, 2006.
[23] B. K. J. Veronica, "An Effective Neural Network Model for Lung Nodule Detection in CT Images with Optimal Fuzzy Model," Multimedia Tools and Applications, vol. 79, pp. 14291–14311, 2020.
[24] B. Nugroho, E. Y. Puspaningrum and A. Yuniarti, "Performance of Face Recognition with Pre-processing Techniques on Robust Regression Method," Int. J. of GEOMATE, vol. 15, no. 50, pp. 101-106, 2018.
[25] I. Khoulqi and N. Idrissi, "Segmentation and Classification of Cervical Cancer," Proc. of the IEEE 6th Int. Conf. on Optimization and Applications (ICOA), pp. 1-7, Beni Mellal, Morocco, 2020.
[26] A. Herbulot, Nonparametric Statistical Measurements for Image and Video Segmentation and Active Contour Minimization, Ph.D. Thesis, University of Nice-Sophia Antipolis, Nice, France, Oct. 2007.
[27] Jiang Xin, R. Zhang and S. Nie, "Image Segmentation Based on Level Set Method," Physics Procedia, vol. 33, pp. 840-845, DOI: 10.1016/j.phpro.2012.05.143, 2012.
[28] F. Chen, "Medical Image Segmentation Using Level Sets," Technical Report, University of Waterloo, Canada, pp. 1-8, 2008.
[29] C. Li, C. Xu, C. Gui and M. D. Fox, "Distance Regularized Level Set Evolution and Its Application to Image Segmentation," IEEE Transactions on Image Processing, vol. 19, no. 12, pp. 3243-3254, 2010.
[30] A. Khadidos, V. Sanchez and C.-T. Li, "Weighted Level Set Evolution Based on Local Edge Features for Medical Image Segmentation," IEEE Trans. on Image Process., vol. 26, no. 4, pp. 1979- 1991, 2017.
[31] J. Bethanney and E. Roslin, "Classification and Detection of Skin Cancer using Hybrid Texture Features," Biomedicine, vol. 37, no. 2, pp.214-22, 2017.
[32] Soumya M., Sneha K. and Arunvinodh C., "Cervical Cancer Detection and Classification Using Texture Analysis, "Biomedical and Pharmacology Journal, vol. 9, no. 2, 2016.
[33] I. Khoulqi and N. Idrissi, "Breast Cancer Image Segmentation and Classification," Proc. of the 4th International Conference on Smart City Applications, pp. 1-9, DOI:10.1145/3368756.3369039, 2019.
[34] S. Paris, "Le Multimédia et la Compression," Lavoisier, Hermes Science Publisher, 1, p. 208, Informatique, Jean-Charles Pomerol, 978-2-7462-2203-8.hal-00841603, 2009.
[35] W. Lin, Z. Wu, L. Lin, A. Wen and J. Li, "An Ensemble Random Forest Algorithm for Insurance Big Data Analysis," IEEE Access, vol. 5, pp. 16568-16575, DOI: 10.1109/ACCESS.2017.2738069, 2017.
[36] I. M. Nasser and S. S. Abu-Naser, "Predicting Tumor Category Using Artificial Neural Networks," International Journal of Academic Health and Medical Research (IJAHMR), vol. 3, no. 2, pp. 1-7, 2019.
[37] R. V. K. Reddy et al., "Prediction of Heart Disease Using Decision Tree Approach," International Journal of Advanced Research in Computer Science and Software Engineering, vol. 6, no. 3, 2016.
[38] L. E. Peterson, "K-nearest Neighbor," Scholarpedia, vol. 4, no. 2, Article ID: 1883, 2009.
[39] C. Krauss, X. A. Do and N. Huck, "Deep Neural Networks, Gradient-boosted Trees, Random Forests: Statistical Arbitrage on the S&P 500, " European Journal of Operational Research, vol. 259, no. 2, pp. 689-702, 2017.
[40] D. Theckedath and R. R. Sedamkar, "Detecting Affect States Using VGG16, ResNet50 and SEResNet50 Networks, "SN Computer Science, vol. 1, Article no. 79, pp. 1-7, 2020.

[41] G. Sun, S. Li, Y. Cao and F. Lang, "Cervical Cancer Diagnosis Based on Random Forest," International Journal of Performability Engineering, vol. 13, no. 4, pp. 446–457, 2017.

[42] D. M. Rouse and S. S. Hemami, "The Role of Edge Information to Estimate the Perceived Utility of Natural Images," Visual Communications Lab., School of Elect. and Comp. Eng., Cornell Uni., 2009.

[43] J. W. Prescott, M. Pennell, T. M. Best et al., "An Automated Method to Segment the Femur for Osteoarthritis Research," Proc. of the Annual International Conference of the IEEE Engineering in Medicine and Biology Society, pp. 6364–6367, DOI: 10.1109/IEMBS.2009.5333257, 2009.

[44] P. K. Malli and S. Nandyal, "Machine Learning Technique for Detection of Cervical Cancer Using KNN and Artificial Neural Network," IJETTCS, vol. 6, no. 4, pp. 145-149, 2017.

[45] K. P. Chandran and U. V. Ratna Kumari, "Improving Cervical Cancer Classification on MR Images Using Texture Analysis and Probabilistic Neural Network," Int. J. of Engineering Sciences & Research Technology, vol. 4, pp. 3141-3145, 2015.

[46] A. I. Naimi and L. B. Balzer, "Stacked Generalization: An Introduction to Super Learning," European Journal of Epidemiology, vol. 33, no. 5, pp. 459-464, 2018.

[47] F. Chollet et al., "Xception: Deep Learning with Depthwise Separable Convolutions," Proc. of the IEEE Conf. on Comp. Vision and Pattern Recog., DOI: 10.1109/CVPR.2017.195, Honolulu, HI, USA, 2017.

[48] T. Majeed et al., "Problems of Deploying CNN Transfer Learning to Detect Covid-19 from Chest Xrays," MedRxiv, DOI: 10.1101/2020.05.12.20098954, 2020.

[49] J. Dekhtiar et al., "Deep Learning for Big Data Applications in CAD and PLM–Research Review, Opportunities and Case Study," Computers in Industry, vol. 100, pp. 227-243, 2018.

[50] K. He, X. Zhang, S. Ren and J. Sun, "Deep Residual Learning for Image Recognition," Proc. of the IEEE Conf. on Computer Vision and Pattern Recog. (CVPR), pp. 770-778, Las Vegas, NV, USA, 2016.

[51] Q. M. Ilyas and M. Ahmad, "An Enhanced Ensemble Diagnosis of Cervical Cancer: A Pursuit of Machine Intelligence towards Sustainable Health," IEEE Access, vol. 9, pp. 12374-12388, 2021.

[52] Akter, Laboni, Md Islam, Mabrook S. Al-Rakhami and Md Haque, "Prediction of Cervical Cancer from Behavior Risk Using Machine Learning Techniques," SN Computer Sci., vol. 2, ID 177, pp. 1-10, 2021.

[53] B. Chitra and S. S. Kumar, "An Optimized Deep Learning Model Using Mutation-based Atom Search Optimization Algorithm for Cervical Cancer Detection," Soft Computing, vol. 25, no. 24, pp. 15363-15376, 2021.

ملخص البحث:

يُعدّ سرطان عُنق الرّحم ثاني أكثر الأمراض الخبيثة شيوعاً لدى النّساء بمعدّل وفيات قدره 60%، ويأتي في طليعة أسباب الوفاة على مستوى العالم. ويُمكن للتّحديد الدّقيق لمراحل المرض أن يُساعد خبراء الأشعّة والأطبّاء في تقديم علاج فعّال عبرالاستفادة من طُرق التّشخيص، مثل صُور الرّنين المغناطيسي. في هذه الورقة، نقترح طريقتيْن؛ تتمثّل الأولى في تقديم آليّ للكشْف المبكّر عن سرطان عُنق الرّحم باستخدام تقنيات معالجة الصّور، وتحليل صُور الرّنين المغناطيسيّ لتحديد المرحلة التي وصل إليها الوَرَم والتّأثير الحقيقي له. وتمرّ عمليّة الكشْف هذه في مراحل ثلاثٍ رئيسيّة (المعالجة الأولية لجعل صُور الرّنين المغناطيسي أسهل للمعالجة والتحليل؛ ثم التّجزئة من أجل استخلاص ما يُسمّى "المناطق ذات الاهتمام"، وفي الخطوة التالية يتم استخلاص فئتيْن من السّمات بناءً على طرقٍ إحصائية وطرق تحويل من أجل وصف صُور الرّنين المغناطيسي). وفي المرحلة النّهائية، تمّ تدريب خمسة مصنِّفات لتصنيف صُور الرّنين المغناطيسي الى صِنفيْن: (حميد وخبيث). أما الطّريقة الثّانية فتهدف الى زيادة أداء الشّبكة العصبية الالتفافيّة العميقة المدرَّبة مسبقاً بناءً على "تعلُّم التّحويل" المستخدَم لتصنيف مجموعات البيانات الخاصّة بالحَوْض لدى النّساء (FP) عن طريق استخدام طريقة التّكديس العامّة التي من شأنها أن توفّر مُصَنِّفاً أكثر فاعلية ومتانةً. وتعدّ زيادة البيانات إحدى طرق المعالجة الأوّلية التي تطبّق على صُور الرّنين المغناطيسي، كما تُستخدم طبقة إسقاطٍ لمنْع الشبكة من فَرْط التّهيئة في مجموعة البيانات الصّغيرة. وقد بينت نتائج التّجريب أنّ زيادة البيانات وتعميم التكديس يعدّان طريقة فعّالة لتحسين معدّل دقّة التّصنيف.